Journal of Power Sources 196 (2011) 8225–8233

Contents lists available at ScienceDirect

Journal of Power Sources

journal homepage: www.elsevier.com/locate/jpowsour

Electrochemical degradation of Nafion ionomer to functionalize carbon support for methanol electro-oxidation

Yu-Chi Hsieh, Jing-Yu Chen, Pu-Wei Wu*

Department of Materials Science and Engineering, National Chiao Tung University, Hsin-chu 300, Taiwan

ARTICLE INFO

Article history:
Received 8 April 2011
Received in revised form 24 May 2011
Accepted 25 May 2011
Available online 24 June 2011

Keywords:
Nafion ionomer
Carbon functionalization
Cyclic voltammetry
Methanol electro-oxidation
Pt

ABSTRACT

An effective electrochemical route to produce functional groups on carbon surface is demonstrated. Cyclic voltammetric (CV) sweeps are performed in 0.5 M H_2SO_4 electrolyte on electrodes containing carbon cloth, Vulcan XC72R, and Nafion ionomer. With supply of ambient oxygen, the generation of hydroxyl radicals from the oxygen reduction reaction during CV cycles initiates the decomposition of Nafion ionomer that leads to formation of oxygenated functional groups on the carbon surface. Ion chromatography confirms the dissolution of sulfate anions upon CV scans. Raman analysis suggests a minor alteration for the carbon structure. However, X-ray photoelectron spectroscopy indicates a significant increase of oxygenated functional groups in conjunction with notable reduction in the fluorine content. The amount of the oxygenated functional groups is determined by curve fitting of C 1s spectra with known constituents. These functional groups can also be found by immersing the as-prepared electrode in a solution containing concentrated residues from Nafion ionomer decomposition. The functionalized electrode allows a 170% increment of Pt ion adsorption as compared to the reference sample. After electrochemical reductions, the functionalized electrode reveals significant improvements in electrocatalytic abilities for methanol oxidation, which is attributed to the oxygenated functional groups that facilitates the oxidation of CO on Pt.

1. Introduction

Carbonaceous materials have been widely used as the substrates for catalyst impregnations in room tempeaturare fuel cells like polymer membrane fuel cells and direct methanol fuel cells [1–10]. It is because with the selection of carbons as supports, nanoparticulate catalysts such as Pt and PtRu are able to distribute uniformly, leading to reduced loading and better catalyst utilization. To date, carbons in a rich variety of forms including carbon blacks, carbon nanotubes (CNTs), mesoporous carbons, carbon nanocapsules, activated carbons, and carbon xerogels have been investigated as the catalyst supports with impressive results [11–16]. The interactions between the carbon and catalyst are critical because a lack of sufficient bonding between them causes possible detachments and colaescence, which results in undesirable performance degradation [17]. Unfortunately, untreated carbons are often hydrophobic in nature that allow poor adsorption of catalyst precursors and catalysts. Therefore, it is necessary to carry out additional functionalization treatments on the carbons to render a hydrophilic surface instead. After proper surface functionalizations, the carbons are expected to adsorb more catalyst precursors for a larger amount of catalyst deposition.

Earlier studies on the carbon functionalizations are concerned with carbon corrosions because under the operation conditions of phosphoric acid fuel cells, the carbon is prone to oxidation loss by the formation of surface oxidized groups [18–22]. In general, the functionalization of carbon involves anodization treatments in concentrated acids at moderate temperature [23,24]. For example, Kangasniemi et al. imposed potentiostatic treatments on the Vulcan XC72 (XC72) in 1 M H_2SO_4 solution, and determined that at room termperature, a signficant oxidation was occurring for the anodizing voltage of 1.2 V for 16 h but 0.8 V was sufficent at 65 °C to produce the same effect [25]. A similar anodization treatment of 2 V was employed by Stevanovic et al. to introduce selective functional groups on the glassy carbons [26]. The degree of surface functionalization also depends on the type of carbon materials because their surface area and microstructure differ considerably. For instance, the CNTs reveal notable oxidation resistance over the XC72 while the BP2000, with a larger specific surface area ($m^2\ g^{-1}$), experiences more oxidation loss as opposed to the XC72 with a smaller specific surface area [27]. So far, after functionalization, surface oxidized groups such as phenols, carbonyls, carboxylic acids, ethers, quinones, and lactones have been identified. The exact mechanism responsible for the formation of selective functional groups is contingent on the processing steps involved and the type

* Corresponding author. Tel.: +886 3 5131227; fax: +886 3 5724727.
E-mail address: ppwu@mail.nctu.edu.tw (P.-W. Wu).

0378-7753/$ – see front matter © 2011 Elsevier B.V. All rights reserved.
doi:10.1016/j.jpowsour.2011.05.068

of carbon materials. Since the carbon is relatively inert in corrosive electrolytes, typical surface functionalization steps are rather time-consuming. Therefore, it is of particular interest to develop a simple and efficient process for functionalization purpose.

An alternative approach to functionalize the carbon materials is by chemical alteration of polymeric binders. In electrode fabrications, Nafion ionomer is often added in mixture with carbons, serving simultaneously as a binder and conductive path for proton transport. Therefore, it is possible that the Nafion ionomer would suffer from structural damage and loss of sulfonic acid side chains if deliberate electrochemical treatments are applied. Previously, extensive efforts have been devoted to understand the responsible mechanism for Nafion membrane degradation in different environments and factors including humidity, temperature, and oxygen concentration are found to be relevant [28,29]. According to literature, hydroxyl (•OH) and peroxy (•OOH) radicals formed during fuel cell operations are able to react with polymer end groups that still contain residual terminal H-groups [30–32]. Further studies indicate that the sulfonic acid side chains are also susceptible to radicals [29,33,34]. In addition, the degraded species of Nafion contain free radicals that have been reported to attack carbons and chemically bond to their surface [35–37]. Moreover, it is suggested that the presence of functionalized groups on the carbon surface is possible to engender additional oxidized groups [38–40]. In light of this information, we realize that the intentional degradation of Nafion ionomer might provide an effective route for carbon functionalization.

In this work, we conducted multiple cyclic voltammetric scans (CV) to introduce functional groups on the electrode structure, followed by Pt cation adsorption and electrochemical reduction to produce nanoparticulate Pt impregrenated on the functionalized support. Electrocatalytic analysis on the methnaol electro-oxidation was performed to elucidate the effect of functionalized support for catalytic actions.

2. Experimental

2.1. Carbon surface functionalization

The electrode for surface functionalization was fabricated by depositing a carbon/Nafion mixture onto a commercially available carbon cloth (E-TEK). First, 10 mg Nafion ionomer solution (5 wt%) and 8 mg carbon powders (Vulcan XC72R) were mixed in 5 mL 99.5 wt% ethanol for 60 min under sonication to form an ink dispersion. The dispersion was deposited repeatedly on a 4 cm^2 carbon cloth which was kept at 80 °C atop a hotplate to evaporate residual solvent. The loadings for the XC72R and Nafion ionomer on the carbon cloth were 2 and 0.125 mg cm^{-2}, respectively. Subsequently, the surface functionalization was performed by imposing CV scans on the electrode (active area of 0.785 cm^2) for 20 cycles between −0.2 and 1.1 V (vs. Ag/AgCl) at 50 mV s^{-1} in an aqueous electrolyte of 0.5 M H_2SO_4. A Pt foil of 10 cm^2 was used as the counter electrode. The duration for the CV scans was 17 min. In order to introduce oxygen during the CV scans, the backside for the electrode was pressed against a stainless steel foil that was partially exposed to the ambient oxygen. A schematic for the cell design is illustrated in Fig. 1. For comparison purpose, we also immersed the as-prepared electrodes in 0.5 M H_2SO_4 or 0.1 M HCl aqueous solution with concentrated residues from Nafion ionomer decomposition to analyze their surface functional groups.

2.2. Electrochemical analysis

The functionalized electrode was immersed in 5 mM H_2PtCl_6 aqueous solution (pH adjusted to 8) at 40 °C. The immersion lasted for 48 h to ensure sufficient adsorption of $PtCl_6^{2-}$. To reduce the adsorbed Pt ions, CV scans were carried out between −0.2 and 0.2 V in 0.5 M H_2SO_4 aqueous solution at 50 mV s^{-1}. To evaluate the electrochemical surface area (ECSA) for the deposited Pt, we conducted CV scans between −0.2 and 0.9 V in 0.5 M H_2SO_4 at 50 mV s^{-1}. The ECSA was estimated by the integrated charge in the hydrogen desorption region. For methanol electro-oxidation, multiple CV scans were performed between −0.2 and 0.9 V at 50 mV s^{-1} in 500 mL aqueous solution of 0.5 M H_2SO_4 and 1 M CH_3OH. The area for the working electrode was 0.785 cm^2. For lifetime determination, chronoamperograms were recorded at 0.5 V for 30 min in 500 mL of 0.5 M H_2SO_4 and 1 M CH_3OH. The Ag/AgCl and Pt foil (10 cm^2) were used as the reference and counter electrodes, respectively. Surface functionalization, $PtCl_6^{2-}$ reduction, ESCA determination, and methanol electro-oxidation were carried out at 26 °C in a three-electrode arrangement using a EG&G 263A potentiostat.

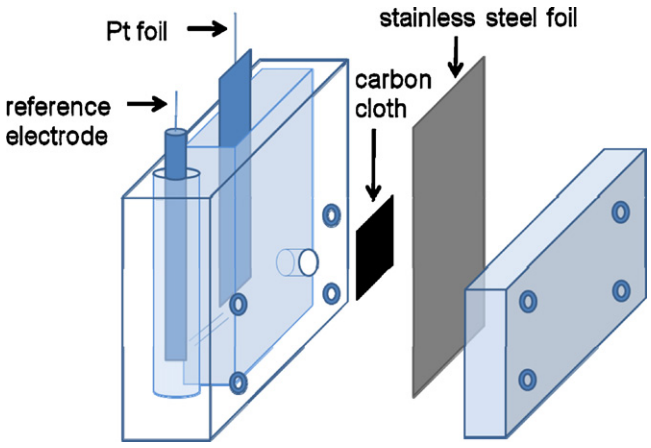

Fig. 1. A schematic of the electrochemical cell for CV scans in 0.5 M H_2SO_4 aqueous solution. The carbon cloth is partially exposed to ambient oxygen.

2.3. Materials characterizations

X-ray Photoelectron Spectroscopy (XPS; Thermo Microlab 350) was adopted to evaluate the oxygenated functional groups on the functionalized electrodes. Raman Spectroscopy (LabRAM HR800) was conducted to detect the microstructure variation on the XC72R after CV scans. Ion chromatography (Dionex DX120) was utilized to analyze the concentration of dissolved SO_4^{2-} and fluorocarbons from the decomposition of Nafion ionomer. Transmission Electron Microscope (TEM; Philips Tecnai-20) was used to observe the morphologies and distributions for the Pt nanoparticles. The average Pt size was obtained by TEM image analysis (Image-Pro Plus 6.0). The amount of Pt loadings was determined by an Inductively Coupled Plasma Mass Spectrometry (ICP-MS; SCIEX ELAN 5000) where the samples were dissolved in a solution containing HCl, HNO_3, and HF at a 2:2:1 volume ratio.

3. Results and discussion

3.1. Electrochemical degradation of Nafion ionomer

Fig. 2 provides the CV profiles at various cycles for the electrodes containing carbon cloth, Nafion ionomer, and XC72R with the supply of ambient oxygen. As shown, the CV profiles exhibited a characteristic behavior for capacitors with symmetric responses in which considerable anodic and cathodic currents were observed above 0.9 V and below −0.1 V, respectively. Notably, the current from the anodic scan for the first cycle was negligible until 0.9 V when a sharp rise occurred. After that, there appeared obvious

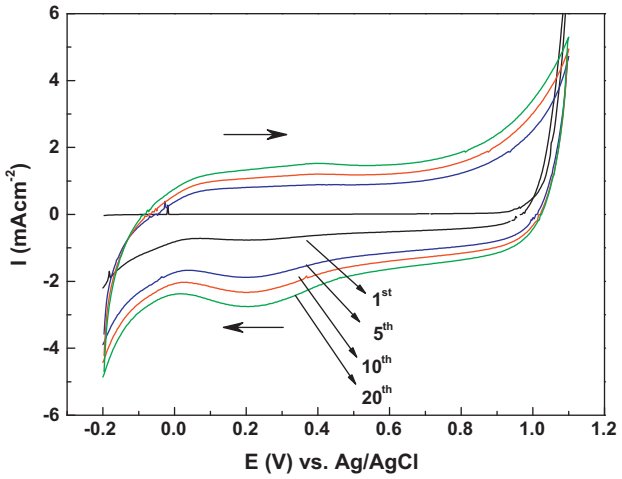

Fig. 2. Profiles from multiple CV scans with ambient oxygen for electrodes containing carbon cloth, XC72R, and Nafion ionomer.

currents for the cathodic scan, suggesting surface activation at an oxidative potential above 0.9 V in the first cycle. Interestingly, both the anodic and cathodic currents demonstrated steady increments with increasing CV cycles. We understood that the recorded currents were mostly from the XC72R as the carbon cloth contributed an insignificant amount with its relatively reduced surface area. However, in our observation, samples of XC72R deposited on the carbon cloth revealed CV curves that were insensitive to increasing cycles, a generic behavior for electrochemical double-layer capacitors. Therefore, we realized that there was chemical degradation of Nafion ionomer that led to the increasing currents.

In order to observe the effect of Nafion ionomer degradation more clearly, we need to remove the capacitive currents from the XC72R. Therefore, we carried out additional experiments with the electrodes containing carbon cloth and Nafion ionomer only. Fig. 3(a) exhibits the CV profiles for the samples with the supply of ambient oxygen. As shown, there appeared obvious oxidation and reduction peaks centering around 0.55 and 0.34 V, respectively. In addition, these signals increased steadily with increasing cycles. According to literature, these peaks were attributed to hydroquinone-quinone redox couple on the carbon substrates, suggesting the formation of oxygenated functional groups on the surface [25–27]. Also shown is the carbon cloth without the addition of Nafion ionomer but with the oxygen supplied from ambient. Obviously, there was negligible current in the CV scans, indicating that without Nafion ionomer, oxygenated functional groups on the carbon surface were not formed at noticeable amount.

Earlier studies on the Nafion membrane degradation have identified the hydroxyl (•OH) and peroxy (•OOH) radicals to be the active species to attack the chemical structure of Nafion. It was suggested that the dissolved oxygen diffuses to the anode side reacting with the hydrogen to form hydrogen peroxide [29,30]. In our case, with sufficient supply of ambient oxygen, the CV scans in an acidic environment on the carbon electrodes were likely to initiate the oxygen reduction reaction by a two-electron route which led to the formation of hydrogen peroxide [41,42]. This hydrogen peroxide subsequently engendered the decomposition of Nafion ionomer that further accelerated the oxidation of carbon. To verify the significance of oxygen in this process, we repeated the experiments with the electrodes containing carbon cloth and Nafion ionomer but without the supply of ambient oxygen. The elimination of oxygen was achieved by immersing the working electrode to the electrolyte completely in a sealed three-electrode cell in conjunction with sufficient argon purging to remove any dissolved oxygen. The resulting CV profiles are displayed in Fig. 3(b). Interestingly, there was negligible difference for the CV responses between the first and 20th cycle, and the hydroquinone–quinone redox couple was rather subdued. This minute amount of redox couple was possibly present in the sample before the CV scans were imposed. According to Fig. 3, without the simultaneous presence of oxygen and Nafion ionomer, the amount of newly formed oxygenated functional groups on the carbon surface was insignificant. An alternative approach to produce the hydroxyl radical (•OH) is the direct oxidation of water [30]. This is a scenario that is possible in the CV scans without the supply of ambient oxygen. However, from Fig. 3(b) we concluded that the direct oxidation of water was unable to produce sufficient hydroxyl radicals (•OH) for Nafion ionomer degradation. Therefore, the principal cause for the formation of oxygenated functionalized groups on the carbon surface was the oxygen reduction route that engendered the decomposition of Nafion ionomer.

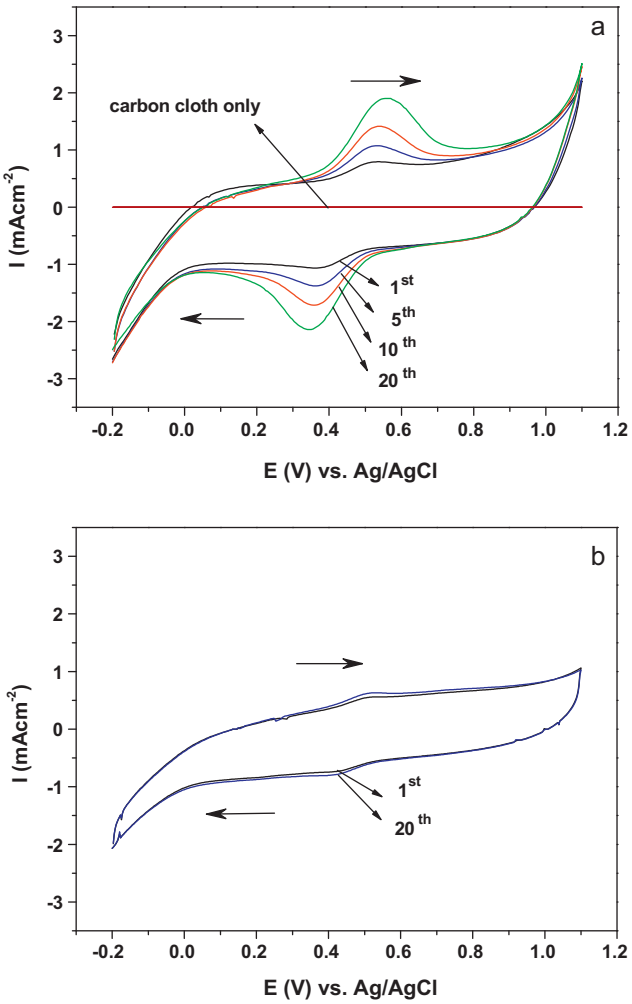

Fig. 3. Profiles from multiple CV scans (a) with ambient oxygen and (b) without ambient oxygen for electrodes containing carbon cloth and Nafion ionomer. Also shown in (a) is the electrode with carbon cloth only.

To further validate the contributory role of Nafion ionomer and oxygen for carbon functionalizations, additional experiments on the carbon cloth and Nafion ionomer were carried out. We performed the CV scans with and without the supply of ambient oxygen, and recorded their anodic currents at the 20th cycle. Fig. 4 exhibits the comparison for the anodic current at 0.5 V for both samples, as well as data from Figs. 2 and 3(a), respectively. Apparently, without the supply of ambient oxygen, the anodic current became relatively subdued for every sample. In general, the presence of oxygen promoted the oxidation of carbon and hence resulted in a larger

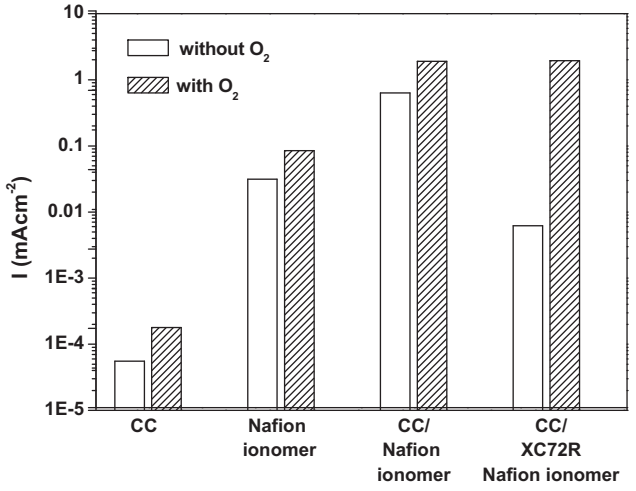

Fig. 4. Comparison in the current value obtained at 0.5 V from the 20th CV cycle for electrodes containing carbon cloth (CC), Nafion ionomer, CC/Nafion ionomer, and CC/XC72R/Nafion ionomer. These CV experiments are performed with ambient oxygen and without ambient oxygen, respectively.

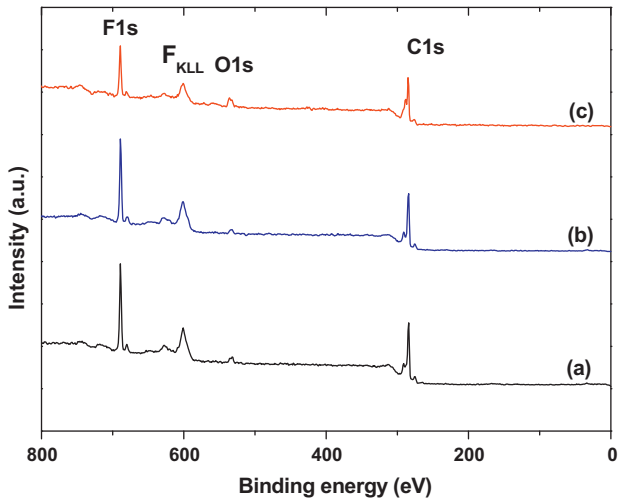

Fig. 6. XPS surveys for (a) as-prepared electrode, as well as electrodes after CV scans (b) without ambient oxygen and (c) with ambient oxygen. These electrodes contain carbon cloth, XC72R, and Nafion ionomer.

oxidation current. However, with the addition of Nafion ionomer, the effect of oxygen became more pronounced. It is therefore concluded that the degradation of Nafion ionomer, promoted by the presence of oxygen, led to accelerated carbon functionalization.

3.2. Carbon functionalization

Fig. 5 demonstrates the Raman spectra for the electrodes after CV scans and H_2SO_4 immersion. As shown, both samples revealed characteristic peaks which were defined as D-band (1310 cm^{-1}) and G-band (1596 cm^{-1}), respectively. The D-band represented the presence of defects and disorder in the carbon structure while the G-band reflected the graphitic in-plane vibrations with E_{2g} symmetry [17]. Hence, the ratio of D/G signals suggested the degree of crystallinity in the carbon structure. As mentioned earlier, the electrode undergoing the H_2SO_4 immersion was selected for comparison purpose and it exhibited a D/G value of 2.57. In contrast, the sample after CV scans revealed a D/G value of 2.67. This moderate variation in the D/G ratio inferred that the carbon structure was reasonably maintained after CV treatments and the formation

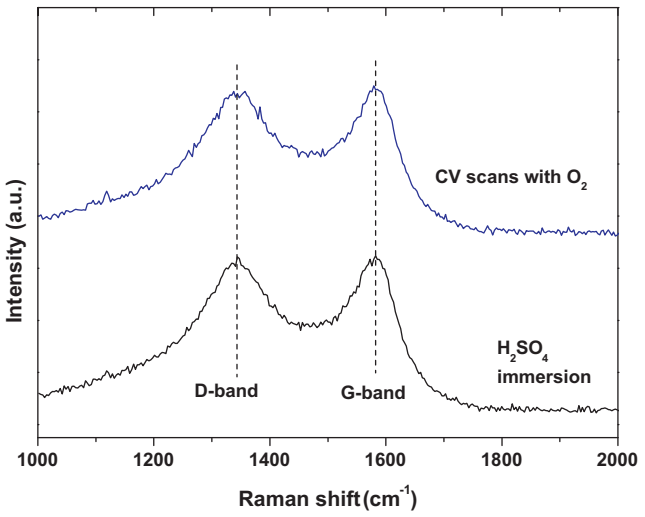

Fig. 5. Raman spectra for electrodes after CV scans with ambient oxygen and H_2SO_4 immersion only. These electrodes contain carbon cloth, XC72R, and Nafion ionomer.

of oxygenated functional groups was caused by the decomposition of Nafion ionomer.

The XPS was adopted to obtain variations on the signals from carbon, oxygen, and fluorine for the electrodes under CV scans with and without the supply of ambient oxygen. We also performed the XPS analysis on the as-prepared electrode without CV scans for comparison. As shown in Fig. 6, relevant peaks on the XPS profiles (resolution in 1 eV) were labeled properly and they were identified as F 1s, F_{KLL}, O 1s, and C 1s, respectively. Table 1 lists their respective atomic ratios. It can be seen that there was negligible difference in the atomic ratios between samples in the as-prepared state and after CV scans without the supply of ambient oxygen. However, the sample after CV scans with the supply of ambient oxygen revealed a similar carbon amount but its atomic ratio for the oxygen was increased considerably in conjunction with a notable reduction in the fluorine content. These results suggested that the CV scans coupled with the supply of ambient oxygen were able to produce oxygen-rich functional groups on the electrode surface while the Nafion ionomer was partially decomposed.

Fig. 7(a) presents the C 1s XPS profiles (resolution in 0.1 eV) for the as-prepared electrode and electrodes after CV scans with and without the supply of ambient oxygen, respectively. Apparently, the as-prepared sample and the one after CV scans without the supply of ambient oxygen displayed similar patterns as expected. In contrast, the sample after CV scans with the supply of ambient oxygen demonstrated a notable peak around 286–288 eV in addition to the typical C 1s signal at 284.5 eV. To understand its nature, this C 1s profile was subjected to curve fitting with known functional groups to determine their relative amounts. Fig. 7(b) illustrates the curve fitting results and the atomic ratios for individual functional groups are listed in Table 2. These functional groups were selected from earlier literature reports and were presumed to be present in the functionalized electrodes [23,25–27]. From Table 2, the sample after CV scans with the supply of ambient oxygen revealed a

Table 1
The atomic ratios for carbon, oxygen, and fluorine from XPS profiles for as-prepared electrode, as well as electrodes after CV scans with and without the supply of ambient oxygen.

	C (at%)	O (at%)	F (at%)
As-prepared	61	4.3	34.7
CV scans without O_2	62	3.5	34.5
CV scans with O_2	61.6	10.5	27.9

Table 2
The atomic ratios for the C–C, –OH, –C=O, –COOH, and C–F from XPS curve fitting for as-prepared electrode, as well as electrodes after CV scans with ambient oxygen and without ambient oxygen.

	C–C (at%) (backbone)	–OH (at%) (a)	–C=O (at%) (b)	–COOH (at%) (c)	C–F (at%)	(a+b+c)/C–C
As-prepared	63.7	14	6.3	5.7	10.3	40.8%
CV scans without O_2	63.7	14	6.3	5	11	39.7%
CV scans with O_2	48	14	20.6	9.1	8.1	91%

notable reduction in the amount for C–F group. In addition, the oxidized –C=O and –COOH groups were substantially increased along with considerable reduction in the C–C backbone.

So far, our results indicated that the decomposition of Nafion ionomer was initiated by the ambient oxygen and this process resulted in the formation of oxygenated functional groups on the carbon surface. To validate our premise, we attempted to obtain the S 2p signal but the 0.5 M H_2SO_4 aqueous solution provided unnecessary background noises. Hence, we prepared several electrodes (carbon cloth/XC72R/Nafion ionomer) and subjected them to CVs in 0.1 M HCl aqueous solution instead. The purpose for these CV scans was to decompose the Nafion ionomer so the HCl solution with concentrated residues was formed. According to Teranishi et al., the degradation of Nafion produced F^-, SO_3^{2-}, CO_2, SO_2, and some fluorocarbons [43]. Subsequently, we immersed the electrode made of XC72R and carbon cloth in the HCl solution containing concentrated Nafion ionomer residues to allow sufficient adsorption of the decomposed species. As shown in Fig. 8, signals from the ion chromatography were attributed to SO_4^{2-} and F^- in different intensities. Similar constituents were observed in earlier work by Chen and Fuller for Nafion membrane degradation [44]. In their work, a rather strong CF_3COO^- peak was identified on the cathode side associated with the oxygen reduction reaction. Unfortunately, in our case the amount of CF_3COO^- was below the detection limit. This notable absence of CF_3COO^- was possibly due to its immediate readsorption onto the carbon surface after detachment from the Nafion backbone.

To monitor the extent of Nafion ionomer degradation, we recorded the signal for SO_4^{2-} upon CV cycles and the resulting data are displayed in Fig. 9. The value for the 0 cycle was obtained from the sample with immersion in the 0.1 M HCl aqueous solution for 17 min, which served as the reference because the sample

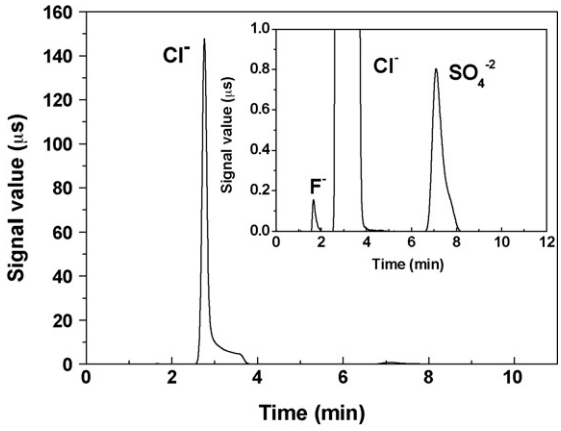

Fig. 8. Ion chromatogram for Nafion ionomer degradation in 0.1 M HCl aqueous solution.

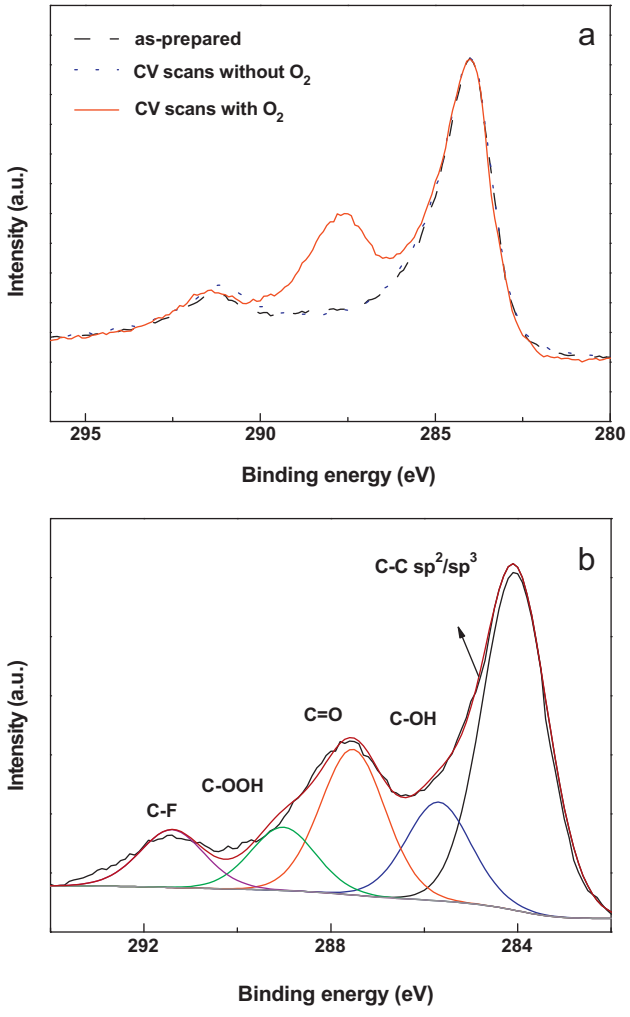

Fig. 7. (a) C 1s XPS profiles for as-prepared electrode, as well as electrodes after CV scans without ambient oxygen and with ambient oxygen. (b) Curve fitting for the C 1s XPS profile from electrode after CV scans with ambient oxygen. These electrodes contain carbon cloth, XC72R, and Nafion ionomer.

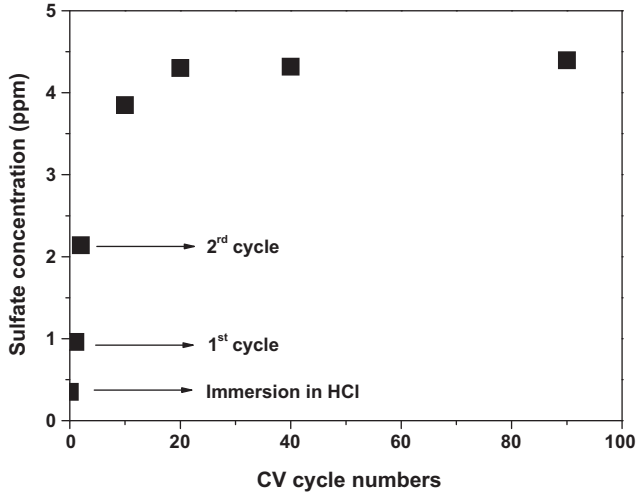

Fig. 9. Variation of sulfate concentration as a function of CV scans with ambient oxygen. The data at 0th cycle is obtained from the electrode immersed in 0.1 M HCl aqueous solution.

Table 3
The atomic ratios for C–C, –OH, –C=O, –COOH, and C–F from C 1s XPS curve fitting for as-prepared electrode, as well as electrodes made of XC72R/carbon cloth with and without immersion in HCl solution containing concentrated residues from Nafion ionomer decomposition.

	C–C (at%) (backbone)	–OH (at%) (a)	–C=O (at%) (b)	–COOH (at%) (c)	C–F (at%)	(a+b+c)/C–C
As-prepared	63.7	14	6.3	5.7	10.3	40.8%
XC72R/carbon cloth without immersion	63.7	17.2	8.3	7	3.8	51%
XC72R/carbon cloth with immersion	46.5	11.6	8.2	27.9	5.8	102.5%

of 20 CV cycles experienced the same amount of time in the 0.5 M H_2SO_4 aqueous solution. As shown, the reference sample revealed sulfate concentration of 0.35 ppm. This reduced amount was not unexpected as the Nafion ionomer likely maintained reasonable chemical stability against the 0.1 M HCl aqueous solution at 26 °C. However, once CV scans were applied, the sulfate anion concentrations became larger considerably reaching a plateau after 20 cycles at 4.3 ppm. Apparently, within the first 20 cycles, there appeared a linear increase in the sulfate concentration with cycling number. This indicated that a desirable amount of Nafion decomposition and its subsequent carbon functionalization was possible by selecting appropriate CV scans.

Fig. 10 provides the C 1s XPS profiles (resolution in 0.1 eV) for the as-prepared electrode (carbon cloth/XC72R/Nafion ionomer) as well as electrodes (carbon cloth/XC72R) with and without immersion in the HCl solution containing concentrated residues from Nafion ionomer decomposition. Apparently, the electrode of XC72R/carbon cloth demonstrated a single C 1s peak at 284 eV while the as-prepared electrode exhibited an additional C–F peak around 291 eV. However, the electrode of XC72R/carbon cloth immersed in the HCl solution with concentrated decomposed Nafion ionomer residues revealed a strong signal around 289 eV which was attributed to the oxygenated groups on the carbon surface. Table 3 lists the atomic ratios for the individual functional groups from the curve fitting results of Fig. 10. Apparently, the sample after immersing in the HCl solution showed a large amount of oxygenated functional groups. We surmised that the Nafion ionomer residue in the HCl solution was likely present as CF_3COO^-. After chemical adsorption, these residues were transformed to the oxygenated functional groups on the carbon surface.

The chemical adsorption of Nafion ionomer residues can also be confirmed from the S 2p XPS profile (resolution in 0.1 eV) displayed in Fig. 11. The electrode of XC72R/carbon cloth revealed a characteristic S 2p signal near 164 eV which was attributed to the impurity intrinsic to the carbon material. However, the electrode of XC72R/carbon cloth/Nafion ionomer demonstrated an additional peak around 168 eV which was caused by the HSO_3 from the Nafion ionomer. Interestingly, the XC72R/carbon cloth sample immersed in the HCl solution with concentrated Nafion ionomer decomposed residues also exhibited the HSO_3 signal in addition to the S 2p from impurity. This further supported our premise that the decomposed Nafion ionomer residues were able to chemically adsorb onto the carbon surface.

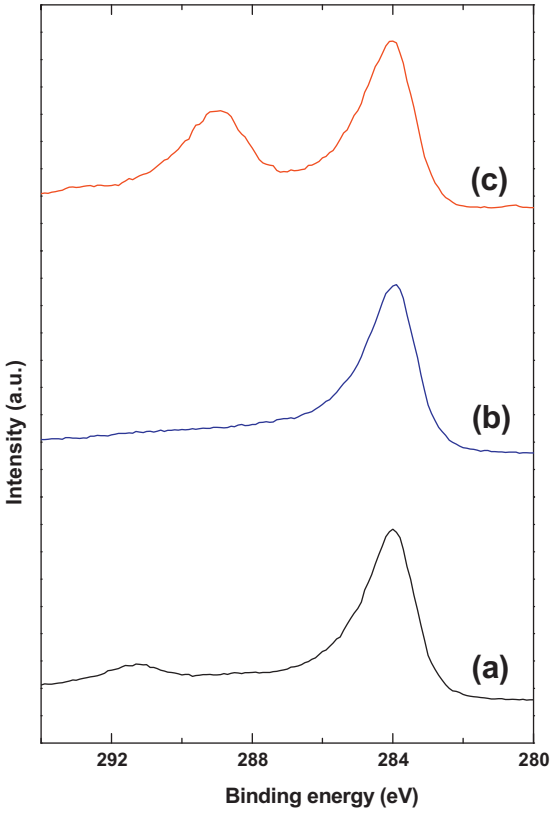

Fig. 10. C 1s XPS profiles for (a) as-prepared electrode (carbon cloth/XC72R/Nafion ionomer), as well as electrodes (carbon cloth/XC72R) (b) before and (c) after immersion in HCl solution containing concentrated residues from Nafion ionomer decomposition.

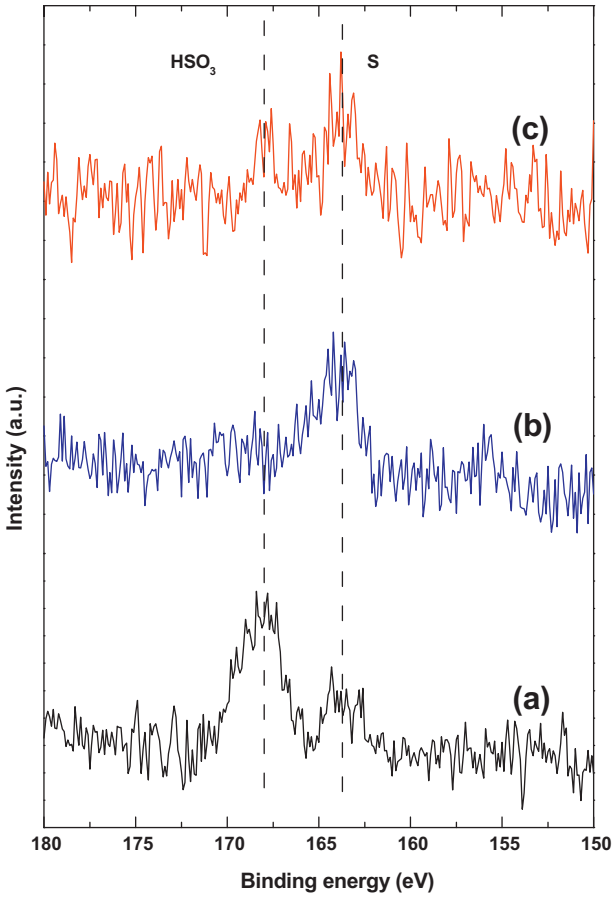

Fig. 11. S 2p XPS profiles for (a) as-prepared electrode (carbon cloth/XC72R/Nafion ionomer), as well as electrodes (carbon cloth/XC72R) (b) before and (c) after immersion in HCl solution containing concentrated residues from Nafion ionomer decomposition.

Table 4
Electrochemical parameters obtained from CV profiles on functionalized and baseline electrodes for methanol electro-oxidation.

	Pt [a] Loading ($\mu g\,cm^{-2}$)	Anodic scan				Cathodic scan			
		V_a [b] mV	i_a [c] $mA\,cm^{-2}$	i_a [d] $mA\,Pt^{-1}\,mg^{-1}$	i_a [e] $mA\,Pt^{-1}\,cm^{-2}$	V_c [f] mV	i_c [g] $mA\,cm^{-2}$	i_c [h] $mA\,Pt^{-1}\,mg^{-1}$	i_c [i] $mA\,Pt^{-1}\,cm^{-2}$
Functionalized electrode	511	729	38.9	76.1	0.47	502	43.7	85.5	0.53
Baseline electrode	301	677	20.4	67.7	0.33	428	19.7	65.4	0.32

[a] total weight of Pt as determined by ICP-MS.
[b] peak potential in anodic scan.
[c] peak apparent current density in anodic scan.
[d] peak mass activity in anodic scan.
[e] peak Pt surface activity in anodic scan.
[f] peak potential in cathodic scan.
[g] peak apparent current density in cathodic scan.
[h] peak mass activity in cathodic scan.
[i] peak Pt surface activity in cathodic scan.

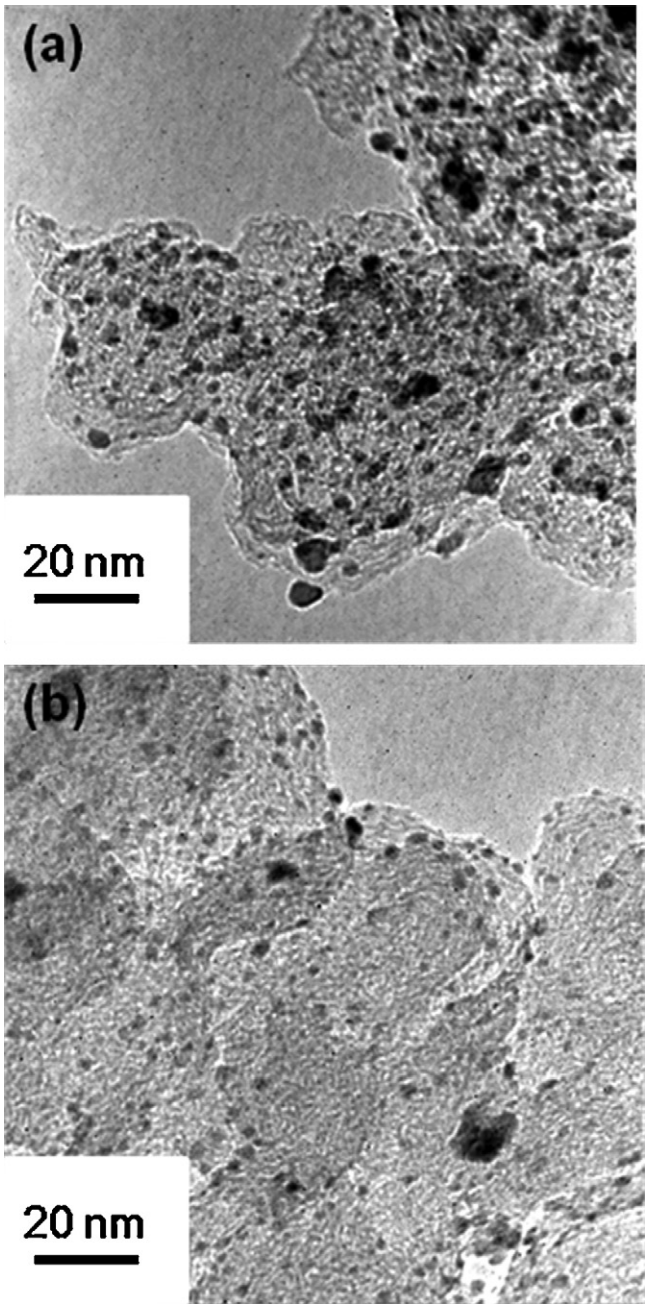

Fig. 12. TEM images for deposited Pt nanoparticles on (a) functionalized and (b) baseline electrodes.

3.3. Methanol electro-oxidation

Fig. 12(a) demonstrates the TEM image for Pt nanoparticles deposited on the functionalized electrode followed by electrochemical reduction. As shown, there were plenty Pt nanoparticles uniformly distributed with notable aggregations. The primary particle size from the image analysis software was 2.68 ± 1.62 nm. The TEM image on the baseline electrode (simple H_2SO_4 immersion followed by electrochemical reduction) is presented in Fig. 12(b). Apparently, the amount of Pt nanoparticles was substantially reduced, a fact consistent with earlier findings from ICP-MS. In addition, their size was slightly smaller at 2.20 ± 1.45 nm. These results confirmed that the functionalized electrode enabled a larger amount of Pt deposits, albeit with moderate coalescence.

Fig. 13 presents the CV profiles of hydrogen desorption and adsorption for the functionalized and baseline electrodes, respectively. As expected, there appeared stronger responses in hydrogen desorption and adsorption for the functionalized electrode because of its relatively larger amount of Pt deposit. Estimation on the ECSA was conducted by the integral area for hydrogen desorption in the anodic scan and the resulting ECSA values were 82.2 and 60.9 cm^2 for the functionalized and baseline electrodes, respectively. This ratio of 1.35 was smaller to that of 1.70 for the Pt loading from ICP-MS. We attributed the reduced ESCA ratio to the observed Pt aggregation on the functionalized electrode.

Fig. 14(a) provides the CV profiles for methanol electro-oxidation in apparent current density for the functionalized and

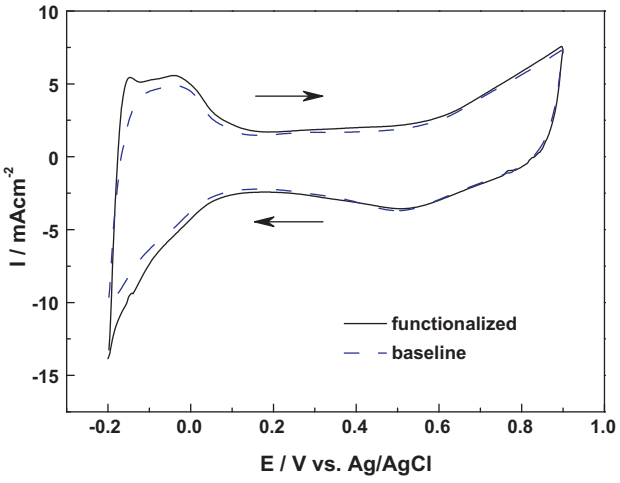

Fig. 13. ECSA profiles for functionalized and baseline electrodes.

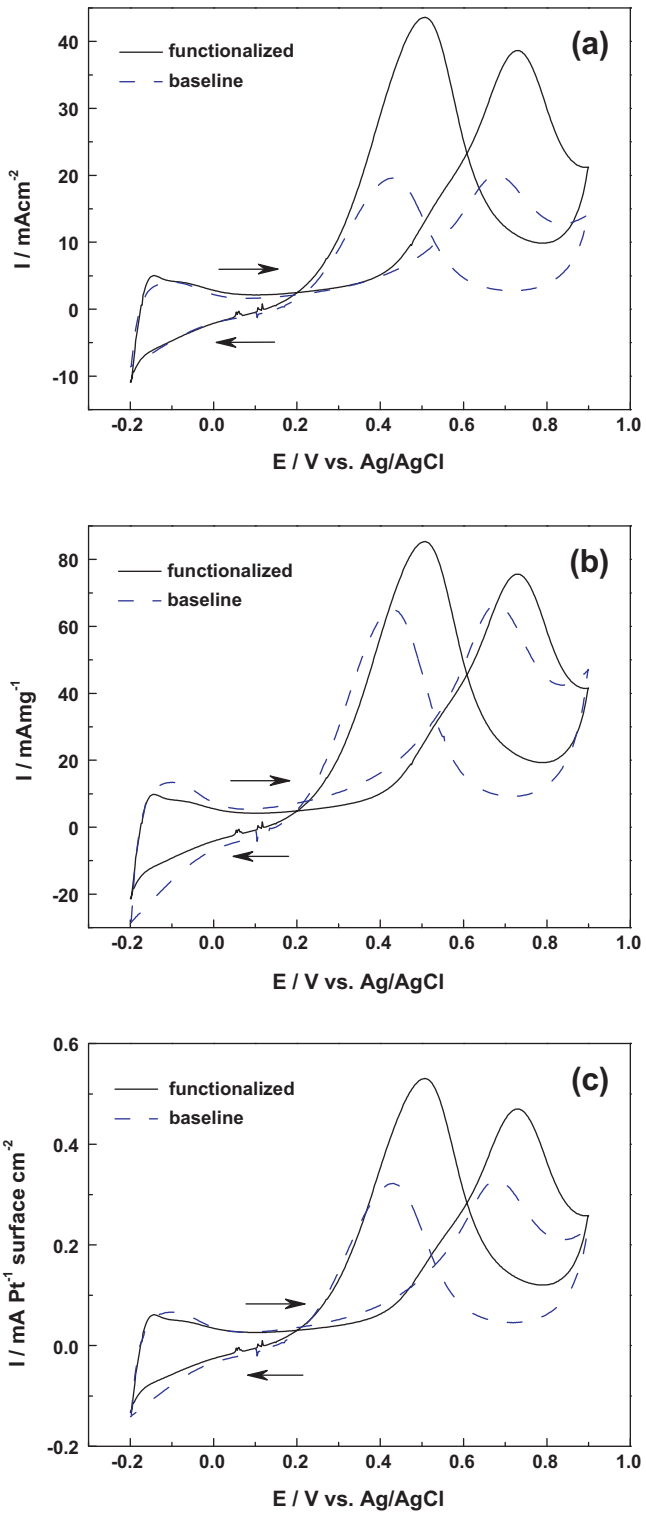

Fig. 14. CV profiles for functionalized and baseline electrodes on methanol electro-oxidation in (a) apparent current density, (b) mass activity, and (c) unit Pt electrochemical surface area.

baseline electrodes, respectively. Relevant electrochemical parameters from these curves are listed in Table 4. According to literature, in these profiles the anodic peak (i_a) is attributed to the oxidation of methanol while the cathodic peak (i_c) corresponds to the oxidation of carbonaceous species produced from earlier methanol oxidation [45–47]. In addition, the ratio (i_a/i_c) indicates the electrocatalytic ability to remove CO. Hence, an electrode with a higher

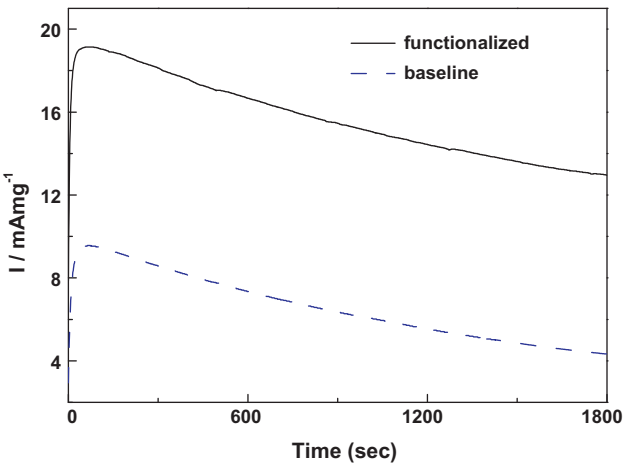

Fig. 15. Chronoamperograms for functionalized and baseline electrodes on methanol electro-oxidation at 0.5 V for 30 min in mass activity.

apparent current and a larger i_a/i_c ratio is always desirable. Notably, the functionalized electrode demonstrated a substantial current increment over that of baseline electrode. This notable improvement was partially caused by a larger Pt deposits which led to a higher nominal current. However, the i_a/i_c ratio for the functionalized electrode was 0.89, which was slightly smaller than 1.03 of baseline electrode. To compare fairly, it is necessary to replot the CV profiles in mass activity and unit Pt ECSA, as shown in Fig. 14(b) and (c). Apparently, there appeared a consistent trend in which the functionalized electrode revealed significant enhancements over that of baseline electrode. These results suggested that the oxygenated functional groups were likely contributing to the methanol electro-oxidation. Similar phenomena were also reported previously in which the oxidized functional groups were believed to provide oxygen-rich species to facilitate CO oxidation on Pt surface [26,48,49].

After confirming enhancements in CVs for the functionalized electrode, it is necessary to evaluate its chronoamperogram for lifetime determination. Fig. 15 provides the chronoamperograms for the functionalized and baseline electrodes at 0.5 V for 30 min in mass activity. Apparently, both electrodes displayed a notable current decay in the first 20 min. However, the amount of current decay was relatively constant for both electrodes and the functionalized electrode was consistently better than the baseline electrode. Since the Pt was used in our study, these performance degradations were not unexpected as poisonous intermediates were able to adsorb on the Pt surface compromising its catalytic ability for methanol oxidation. It is noted that similar behaviors were also observed by Ma et al. in their study of Pt–Ru$(O_xH_y)_m$ electrocatalysts [50].

So far, our work demonstrates a facile approach to functionalize catalyst supports without involving high temperature and large anodic potentials. Since the Nafion ionomer itself is often used as a binder in electrode fabrication, a simple CV with dissolved oxygen nearby could decompose the Nafion ionomer partially resulting in the formation of oxygenated functional groups. These functional groups are active in assisting the Pt for methanol electro-oxidation. It is noted that the enhancement effect observed in this work is different from conventional approaches in which the role of Nafion ionomer is to extend the interfacial area between the Nafion ionomer and electrocatalyst [51]. Moreover, the functional groups could potentially enable a larger electrocatalyst impregnation leading to an improved stability [52]. Further studies are under way to explore the anchoring effect for the functionalized groups and life time performances of supported Pt electrocatalyst.

4. Conclusions

We conducted multiple CV scans in an acidic electrolyte on the electrodes containing carbon cloth, XC72R, and Nafion ionomer. With the supply of ambient oxygen, the Nafion ionomer experienced chemical attacks leaving decomposed residues which were able to adsorb onto the carbon surface leading to an accelerated formation of oxygenated functional groups. The decomposition of Nafion ionomer was attributed to the hydrogen peroxide produced from the oxygen reduction reaction during CV scans. Raman analysis on the carbon electrodes revealed minor structural modification after CV scans. Results from XPS surveys indicated a significant increase of the oxygenated functional groups on the carbon surface in conjunction with a notable reduction in fluorine content. The functionalized electrode was determined to allow a larger amount of Pt ion adsorption as compared to the baseline electrode. After electrochemical reduction, the Pt nanoparticles were evenly formed on the carbon supports. Electrochemical analysis on the methanol electro-oxidation was performed and we observed significant increments in apparent current density, mass activity, as well as unit Pt ESCA for the functionalized electrode.

Acknowledgement

The authors are grateful to Professor Chuen-Jinn Tsai and Miss Yi-Lin Liu from the Institute of Environmental Engineering for their kind assistance with the laboratory equipment. Financial supports from National Science Council of Taiwan (NSC-96-2221-E-009-110) and National Synchrotron Radiation Research Center (2009-2-063-1) are acknowledged.

References

[1] A.L. Dicks, J. Power Sources 156 (2006) 128–141.
[2] M.S. Saha, A. Kundu, J. Power Sources 195 (2010) 6255–6261.
[3] J.F. Drillet, H. Bueb, R. Dittmeyer, U. Dettlaff-Weglikowska, S. Roth, J. Electrochem. Soc. 156 (2009) F137–F144.
[4] J.H. Kim, B. Fang, S.B. Yoon, J.S. Yu, Appl. Catal. B 88 (2009) 368–375.
[5] J.F. Lin, V. Kamavaram, A.M. Kannan, J. Power Sources 195 (2010) 466–470.
[6] A. Guha, T.A. Zawodzinski, D.A. Schiraldi, J. Power Sources 195 (2010) 5167–5175.
[7] N. Spataru, X.T. Zhang, T. Spataru, D.A. Tryk, A. Fujishima, J. Electrochem. Soc. 155 (2008) B264–B269.
[8] V. Baglio, A. Di Blasi, C. D'Urso, V. Antonucci, A.S. Arico, R. Ornelas, D. Morales-Acosta, J. Ledesma-Garcia, L.A. Godinez, L.G. Arriaga, L. Alvarez-Contreras, J. Electrochem. Soc. 155 (2008) B829–B833.
[9] N.Y. Hsu, C.C. Chien, K.T. Jeng, Appl. Catal. B 84 (2008) 196–203.
[10] S. Maass, F. Finsterwalder, G. Frank, R. Hartmann, C. Merten, J. Power Sources 176 (2008) 444–451.
[11] W. Phompan, N. Hansupalak, J. Power Sources 196 (2011) 147–152.
[12] Y.F. Hsieh, Y.C. Hsieh, P.W. Wu, C.H. Liao, Y.M. Chang, J. Electrochem. Soc. 157 (2010) B39–B44.
[13] J.R.C. Salgado, F. Alcaide, G. Alvarez, L. Calvillo, M.J. Lazaro, E. Pastor, J. Power Sources 195 (2010) 4022–4029.
[14] Y.M. Chang, Y.C. Hsieh, P.W. Wu, Diamond Relat. Mater. 18 (2009) 501–504.
[15] R.I. Jafri, T. Arockiados, N. Rajalakshmi, S. Ramaprabhu, J. Electrochem. Soc. 157 (2010) B874–B879.
[16] B. Liu, S. Creager, J. Power Sources 195 (2010) 1812–1820.
[17] G.X. Zhang, S.H. Sun, D.Q. Yang, J.P. Dodelet, E. Sacher, Carbon 46 (2008) 196–205.
[18] P.L. Antonucci, F. Romeo, M. Minutoli, E. Alderucci, N. Giordano, Carbon 26 (1988) 197–203.
[19] N. Giordano, P.L. Antonucci, E. Passalacqua, L. Pino, A.S. Arico, K. Kinoshita, Electrochim. Acta 36 (1991) 1931–1935.
[20] E. Passalacqua, P.L. Antonucci, M. Vivaldi, A. Patti, V. Antonucci, N. Giordano, K. Kinoshita, Electrochim. Acta 37 (1992) 2725–2730.
[21] S.I. Pyun, E.J. Lee, T.Y. Kim, S.J. Lee, Y.G. Ryu, C.S. Kim, Carbon 32 (1994) 155–159.
[22] A.M. Puziy, O.I. Poddubnaya, V.N. Zaitsev, O.P. Konoplitska, Appl. Surf. Sci. 221 (2004) 421–429.
[23] Z.R. Yue, W. Jiang, L. Wang, S.D. Gardner, C.U. Pittman, Carbon 37 (1999) 1785–1796.
[24] R. Berenquer, J.P. Marco-Lozar, C. Quijada, D. Cazorla-Amoros, E. Morallon, Carbon 47 (2009) 1018–1027.
[25] K.H. Kangasniemi, D.A. Condit, T.D. Jarvi, J. Electrochem. Soc. 151 (2004) E125–E132.
[26] S. Stevanovic, V. Panic, D. Tripkovic, V.M. Jovanovic, Electrochem. Commun. 11 (2009) 18–21.
[27] J.J. Wang, G.P. Yin, Y.Y. Shao, S. Zhang, Z.B. Wang, Y.Z. Gao, J. Power Sources 171 (2007) 331–339.
[28] C. Chen, T.F. Fuller, J. Electrochem. Soc. 156 (2009) B1218–B1224.
[29] C. Chen, G. Levitin, D.W. Hess, T.F. Fuller, J. Power Sources 169 (2007) 288–295.
[30] F.A. de Bruijn, V.A.T. Dam, G.J.M. Janssen, Fuel Cells 8 (2008) 3–22.
[31] D.A. Schiraldi, Polym. Rev. 46 (2006) 315–327.
[32] D.E. Curtin, R.D. Lousenberg, T.J. Henry, P.C. Tangeman, M.E. Tisack, J. Power Sources 131 (2004) 41–48.
[33] G. Hubner, E. Roduner, J. Mater. Chem. 9 (1999) 409–418.
[34] T. Xie, C.A. Hayden, Polymer 48 (2007) 5497–5506.
[35] H.P. Boehm, Carbon 32 (1994) 759–769.
[36] A. Bravo, H.R. Bjorsvik, F. Fontana, L. Liguori, A. Mele, F. Minisci, J. Org. Chem. 62 (1997) 7128–7136.
[37] M. Sansotera, C.L. Bianchi, G. Lecardi, G. Marchionni, P. Metrangolo, G. Resnati, W. Navarrini, Chem. Mater. 21 (2009) 4498–4504.
[38] J. Xie, D.L. Wood, K.L. More, P. Atanassov, R.L. Borup, J. Electrochem. Soc. 152 (2005) A1011–A1020.
[39] T. Morimoto, K. Hiratsuka, Y. Sanada, K. Kurihara, J. Power Sources 60 (1996) 239–247.
[40] C.T. Hsieh, H. Teng, Carbon 40 (2002) 667–674.
[41] K. Kinoshita, Oxygen electrochemistry, in: Electrochemical Oxygen Technology, John Wiley & Sons, New York, 1992, pp. 21–26.
[42] C. Chen, T.F. Fuller, Electrochim. Acta 54 (2009) 3984–3995.
[43] K. Teranishi, K. Kawata, S. Tsushima, S. Hirai, Electrochem. Solid-State Lett. 9 (2006) A475–A477.
[44] C. Chen, T.F. Fuller, Polym. Degrad. Stab. 94 (2009) 1436–1447.
[45] T.C. Deivaraj, J.Y. Lee, J. Power Sources 142 (2005) 43–49.
[46] Z.B. Wang, G.P. Yin, J. Zhang, Y.C. Sun, P.F. Shi, Electrochim. Acta 51 (2006) 5691–5697.
[47] Z.L. Liu, X.Y. Ling, B. Guo, L. Hong, J.Y. Lee, J. Power Sources 167 (2007) 272–280.
[48] J.H. Chen, M.Y. Wang, B. Liu, Z. Fan, K.Z. Cui, Y. Kuang, J. Phys. Chem. B 110 (2006) 11775–11779.
[49] M.A. Scibioh, I.H. Oh, T.H. Lim, S.A. Hong, H.Y. Ha, Appl. Catal. B 77 (2008) 373–385.
[50] J.H. Ma, Y.Y. Feng, J. Yu, D. Zhao, A.J. Wang, B.Q. Xu, J. Catal. 275 (2010) 34–44.
[51] C.H. Park, M.A. Scibioh, H.J. Kim, I.H. Oh, S.A. Hong, H.Y. Ha, J. Power Sources 162 (2006) 1023–1028.
[52] W.M. Chen, Q. Xin, G.Q. Sun, Q. Wang, Q. Mao, H.D. Su, J. Power Sources 180 (2008) 199–204.